

This research has been supported in part by the Swedish Natural Science Research Council (NFR) and in part by the United States Office of Naval Research under Contract no. N00014-81-K-0526. We are also grateful to our laboratory technician Hilding Karlsson for his skilled assistance.

References

- BLESSING, R. H., COPPENS, P. & BECKER, P. (1974). *J. Appl. Cryst.* **7**, 488–492.
- BOILOT, J. P., COLOMBAN, P., COLLIN, G. & COMÈS, R. (1980). *J. Phys. Chem. Solids*, **41**, 47–54.
- BOILOT, J. P., COLOMBAN, P., COLLONGUES, R., COLLIN, G. & COMÈS, R. (1980). *J. Phys. Chem. Solids*, **41**, 253–258.
- BRUCE, J. A., HOWIE, R. A. & INGRAM, M. D. (1986). *Solid State Ionics*, **18–19**, 1129–1133.
- CATTI, M., CAZZANELLI, E., IVALDI, G. & MARIOTTO, G. (1987). *Phys. Rev. B*, **36**, 9451–9460.
- EDSTRÖM, K., THOMAS, J. O. & FARRINGTON, G. C. (1988). *Solid State Ionics*, **28–30**, 363–368.
- EDSTRÖM, K., THOMAS, J. O. & FARRINGTON, G. C. (1991). *Acta Cryst.* **B47**, 635–643.
- LEHMANN, M. S. & LARSEN, F. K. (1974). *Acta Cryst.* **A30**, 580–584.
- LUNDGREN, J.-O. (1982). *Crystallographic Computer Programs*. Report UUIC-B13-04-05. Institute of Chemistry, Univ. of Uppsala, Sweden.
- MCCANDLISH, L. E., STOUT, G. H. & ANDREWS, L. C. (1975). *Acta Cryst.* **A31**, 245–249.
- REIDINGER, F. (1979). PhD Thesis, State Univ. of New York, Albany, USA.
- ROTH, W. L. (1972). *J. Solid State Chem.* **4**, 60–75.
- ROTH, W. L., REIDINGER, F. & LAPLACA, S. (1976). *Superionic Conductors*, edited by G. D. MAHAN & W. L. ROTH, pp. 223–241. New York: Plenum Press.
- SUTTER, P. H., CRATTY, L., SALTZBERG, M. & FARRINGTON, G. C. (1983). *Solid State Ionics*, **9–10**, 295–298.
- TOFIELD, B. C. & FARRINGTON, G. C. (1979). *Nature (London)*, **278**, 438–439.
- YAO, Y. F. & KUMMER, J. T. (1967). *J. Inorg. Nucl. Chem.* **29**, 2453–2474.

Acta Cryst. (1991). **B47**, 650–659

Charge Densities in CoS₂ and NiS₂ (Pyrite Structure)

BY ELLEN NOWACK

Institut für Kristallographie, RWTH Aachen, Templergraben 55, D-5100 Aachen, Germany

DIETER SCHWARZENBACH

Institut de Cristallographie, Université de Lausanne, Bâtiment des Sciences Physiques, Dorigny, CH-1015 Lausanne, Switzerland

AND THEO HAHN

Institut für Kristallographie, RWTH Aachen, Templergraben 55, D-5100 Aachen, Germany

(Received 23 November 1990; accepted 22 April 1991)

Dedicated to Professor Karl Fischer on the occasion of his 65th birthday

Abstract

The electron-density distributions in the pyrite-type structures of CoS₂ and NiS₂ have been determined from high-resolution single-crystal diffraction data [Ag K α radiation; resolution and temperature (sin θ / λ)_{max} = 1.49 Å⁻¹ at 295 K for CoS₂, 1.63 Å⁻¹ at 135 K for NiS₂]. The charge densities were refined using a multipolar deformation model [$R(|F|)$ = 0.0119 and 0.0136, respectively]. The X-ray diffraction data of FeS₂ [Stevens, DeLucia & Coppens (1980). *Inorg. Chem.* **19**, 813–820; Ag K α radiation, (sin θ / λ)_{max} = 1.46 Å⁻¹, room temperature] were refined using the same deformation model and program in order to facilitate comparison of the results [$R(|F|)$ = 0.0176]. The main features of the result-

ing deformation maps agree well for all three structures. They consist of important maxima in the immediate vicinity of the metal atoms pointing towards the faces of the coordination octahedron. The heavier the metal atom, the smaller is the distance of the maxima from the atomic centre. These features are interpreted by a preferential occupation of the metal *d* orbitals which correspond to the cubic *t*_{2g} orbitals. An analysis of the *d*-orbital populations indicates that the symmetry of the electron distribution around the metal atom is in all cases very close to cubic, the site symmetry being $\bar{3}$; the *t*_{2g} orbitals appear to be fully occupied by six electrons while the occupation of the *e*_g orbitals increases in the series Fe, Co, Ni and indicates covalent overlap with the S ligands.

Introduction

The transition-metal disulfides MS_2 ($M = \text{Mn, Fe, Co, Ni, Cu, Zn}$) crystallize in the cubic pyrite structure which is related to the NaCl structure. The space group is $Pa\bar{3}$ (No. 205). The metal atoms occupy the Na sites [M : Wyckoff position $4(a)$, $\bar{3}$, 000], and S_2 pairs are located at the Cl sites [S : Wyckoff position $8(c)$, $3, xxx$], $Z = 4$. The axes of the four S_2 pairs in the unit cell are oriented along the four $\langle 111 \rangle$ directions. Each cation is surrounded by six nearest-neighbour anions which form a trigonally distorted octahedron, whereas each anion is coordinated to three cations and one anion, forming a distorted tetrahedron.

The atoms of the S_2 dumbbells are linked by a strong covalent σ bond. In contrast, the metal-sulfur bond is assumed to be essentially ionic with a significant covalent contribution in FeS_2 , CoS_2 , NiS_2 , CuS_2 and ZnS_2 , and predominantly ionic in MnS_2 . The transition-metal atoms with formal valence +2 have $3d^5$ to $3d^{10}$ configurations. The d levels are split by the octahedral crystal field into e_g and t_{2g} orbitals; the latter are further split into an a_g and an e'_g level as a result of the trigonal distortion of the coordination octahedron. In MnS_2 , Mn^{2+} assumes the high-spin configuration and all d electrons are localized on the metal ion. For the other cations in the series, low-spin arrangements have to be assumed. The t_{2g} states are essentially localized and non-bonding. Slight covalent mixing of the metal e_g with the S $3p$ orbitals results in the formation of narrow bands of width 0.5 to 1.0 eV (Bullett, 1982; Lauer, Trautwein & Harris, 1984) which are well separated from the t_{2g} states. The anion-cation bonding σ band has substantial sulfur $3p$ character, the antibonding σ^* band has metal d character and is therefore denoted as e_g^* .

The variation of the electrical and magnetic properties in the series of compounds FeS_2 to ZnS_2 has been ascribed to the increasing number of electrons in the antibonding e_g^* band (e.g. Bither, Bouchard, Cloud, Donohue & Siemons, 1968; Goodenough, 1971; Vaughan & Craig, 1978). FeS_2 is a diamagnetic semiconductor with a band gap of ~ 0.95 eV (Schlegel & Wachter, 1976) between the t_{2g} states and the empty e_g^* band. CoS_2 is ferromagnetic and has metallic conductivity. The e_g^* band containing one electron is quarter filled; the band is narrow enough to permit magnetic ordering, even though it has a reduced moment. NiS_2 is an antiferromagnetic semiconductor. Its half-filled e_g^* band is split into spin-up and spin-down sub-bands due to electron repulsion, opening a band gap of ~ 0.27 eV (Kautz, Dresselhaus, Adler & Linz, 1972), and only the spin-up sub-band is filled. Thus, NiS_2 is a Mott insulator (Mott, 1961; Hubbard, 1964). Increasing the pressure to 30–40 kbar or alloying with NiSe_2

induces a transition into the metallic state (Wilson & Pitt, 1971). Metallic properties are also developed by introducing vacancies in the nickel substructure (Krill, Lapiere, Gautier, Robert, Czjzek, Fink & Schmidt, 1976). CuS_2 is metallic and superconducting ($T_c < 1.5$ K) and exhibits temperature-independent paramagnetism; three electrons are contained in a single e_g^* band. ZnS_2 is a diamagnetic semiconductor, all its d bands are filled.

The successive filling of the antibonding e_g^* bands in proceeding from FeS_2 to CuS_2 is correlated with variations in the M —S bond lengths which are 2.26, 2.31, 2.40 and 2.45 Å for FeS_2 , CoS_2 , NiS_2 and CuS_2 , respectively (King & Prewitt, 1979). The effective ionic radii of the M^{2+} ions are 0.61, 0.65, 0.69 and 0.73 Å, respectively (Shannon, 1976). Thus, the increase in the M —S bond lengths is larger than the increase of the ionic radii. This indicates decreasing metal-sulfur interaction with increasing number of d electrons. Since bonding interactions between metal and S result in some depletion of the electron density in the S—S pairs, the tendency of decreasing M —S interactions is accompanied by an increase in the S—S bond strength and consequently by a shortening of the S—S bond lengths (2.15, 2.12, 2.06 and 2.03 Å, respectively) (Kjekshus & Nicholson, 1971). All S—S distances are larger or of the order of magnitude of the single-bond distance in the S_8 molecule (2.05 Å). The structure of ZnS_2 has not been determined.

The electron-density distribution of FeS_2 with the pyrite structure has been determined by Stevens, DeLucia & Coppens, (1980). The present study presents the deformation densities of CoS_2 and NiS_2 , determined experimentally from high-resolution X-ray diffraction data. In order to facilitate comparison with the results for FeS_2 , the deposited diffraction data of Stevens *et al.* (1980) were refined with our charge-density least-squares program *LSEXP* using exactly the same functional base as for CoS_2 and NiS_2 .

Experimental

Crystals of both CoS_2 and NiS_2 were grown by chemical transport with Cl_2 as transporting medium by Krabbes & Oppermann (1984) and Kikuchi, Miyadai, Fukui, Itô & Takizawa (1978). They have kindly been supplied to us by the authors. Spherical specimens were prepared with a crystal grinder according to Bond (1951). From these, untwinned and non-intergrown crystals, as checked by precession photographs, were selected for data collection.

The structure factors of the pyrite structure fall into the following classes according to the parities of the indices hkl : for h, k, l all even or all odd, all atoms contribute; for h, k, l with mixed parities, only

the S atoms contribute. Thus, in general, the reflections with unmixed indices are dominated by the metal atoms and have high intensities, whereas the reflections with mixed indices are weaker.

Intensity measurements on CoS₂ and NiS₂ (Table 1) were carried out on Enraf-Nonius CAD-4 diffractometers with Ag K α radiation ($\lambda\bar{\alpha} = 0.56087 \text{ \AA}$) using a graphite (002) monochromator. The data set for NiS₂ was collected at the reduced accelerating voltage of 45 kV in order to avoid contributions of $\lambda/2$ radiation which would mainly contaminate the intensities of reflections with mixed indices; this would lead to biased results and in particular to a biased site-occupancy parameter for S. This aspect is more important for NiS₂ since, in contrast to CoS₂, a range of nonstoichiometric compositions is known. The lattice parameter is a measure of the nickel vacancy concentration (Krill *et al.*, 1976) and special care was therefore taken to determine its value precisely. For this purpose, the 2θ angles of 40 reflections in the range $44 < 2\theta < 82^\circ$ were measured on both sides of the primary beam. The least-squares refinement using the resulting 2θ values led to a lattice parameter of 5.6852 \AA (Table 1) which corresponds to the composition NiS_{1.97}. According to Krill *et al.* (1976), NiS_{*x*} in the range $1.91 \leq x \leq 2.1$ has a nearly constant S-vacancy concentration of about 4%, the variation in *x* being due to Ni vacancies. The Ni-vacancy concentration of the particular crystal used in our experiments is therefore about 2.7%.

The data set of CoS₂ was collected at room temperature, whereas the NiS₂ measurements were taken at 135 K using a nitrogen gas-flow cooling device (Enraf-Nonius). The temperature fluctuations near the nozzle, inside the Dewar tube, were less than 1 K. All symmetry-equivalent reflections within a full sphere of reciprocal space were measured for CoS₂ ($-14 \leq h \leq 14$, $-14 \leq k \leq 14$, $-16 \leq l \leq 14$) and within half a sphere for NiS₂ ($0 \leq h \leq 18$, $-18 \leq k \leq 18$, $-18 \leq l \leq 18$).

Reflection profiles of both compounds were rather broad indicating a large mosaic spread. Therefore, the full profiles of all reflections were stored in the output file. They were subsequently checked for overlapping profiles of neighbouring reflections, but no such overlap was found. Reflections which were clearly affected by multiple diffraction, as indicated by measurements at different ψ angles, and reflections with obviously disturbed profiles were eliminated. Backgrounds were estimated by using the standard background-correction procedure of the CAD-4 diffractometer program which assumes the first and last sixths of the scan to be background. Three intensity-control reflections were measured, for CoS₂ every 10000 s, for NiS₂ every 6000 s. The variance of an intensity was computed according to

Table 1. *Data collection*

	CoS ₂	NiS ₂
Location of diffractometer	Aachen	Lausanne
Diameter of crystal spheres (mm)	0.165	0.200
μR	0.52	0.62
Temperature (K)	295	135
Voltage (kV), current (mA)	56, 20	45, 26
Scan mode	$\omega - 2\theta$	$\omega - \frac{1}{2}\theta$, $\theta \leq 20^\circ$ $\omega - 2\theta$, $\theta > 20^\circ$
Scan angle ω (°)	$2.60 + 1.00 \tan \theta$	$2.80 + 0.45 \tan \theta$
Aperture horizontal (°)	0.48–1.14	1.41–1.97
Scan speed ω (° min ⁻¹)	4.0–6.0	2.5
($\sin \theta / \lambda$) _{max} (\AA^{-1})	1.49	1.63
Number of measured reflections	14 834	14 370
Number of independent reflections*	743, 545	1113, 762
Absorption min., max.	1.998, 2.124	2.214, 2.475
$R_{int}(I)$	0.0442	0.0449
a (135 K) (\AA)	—	5.6765 (1)
a (295 K) (\AA)	5.5385 (2)	5.6852 (2)

* All data and those with $I > 3\sigma(I)$, respectively.

$\sigma^2(I) = \sigma^2(\text{counting statistics}) + (KI)^2$ where K was obtained by analysing the fluctuations of the control reflections about their mean values. For CoS₂ and NiS₂, K amounted to 0.021 and 0.004, respectively. The data set for NiS₂ was corrected for scan truncation according to Denne (1977). Absorption factors [$\mu(\text{CoS}_2) = 62.53$, $\mu(\text{NiS}_2) = 62.46 \text{ cm}^{-1}$] and absorption-weighted mean-path lengths for the spheres were taken from Dwiggin (1975) and Flack & Vincent (1978).

For the intensities I_i in each set of symmetry-equivalent reflections, the unweighted mean intensity \bar{I} was computed. For the variance of \bar{I} , the larger of the two quantities $\sigma_1^2(\bar{I}) = \sum \sigma^2(I_i) / n^2$ and $\sigma_2^2(\bar{I}) = \sum (\bar{I}_i - \bar{I})^2 / n(n-1)$ was chosen, where n is the number of measurements in each set. Most σ_2 values are smaller than $1.5\sigma_1$ except for some low-order reflections. Following an argument of Bayesian statistics (French & Oatley, 1982), negative mean intensities were set to zero.*

All data-reduction calculations were carried out with programs developed at Lausanne and incorporated in the XRAY system (Stewart, Kruger, Ammon, Dickinson & Hall, 1972).

Least-squares refinements

The charge-density refinement program *LSEXP* used in this work is described by Restori & Schwarzenbach (1986). In addition to the standard procrystal model defined by positional and anisotropic displacement parameters, population parameters of the atomic sites, scale factor and secondary-extinction parameters (Becker & Coppens, 1974, 1975), the program provides a representation

* Lists of structure factors have been deposited with the British Library Document Supply Centre as Supplementary Publication No. SUP 54183 (18 pp.). Copies may be obtained through The Technical Editor, International Union of Crystallography, 5 Abbey Square, Chester CH1 2HU, England.

Table 2. Standard structural parameters and reliability indices

Definition: the scale factor is defined by $F_o = \text{scale} \times y \times F_{\text{corr}} \approx \text{scale} \times F_c$, y being the extinction correction. The extinction parameter G refers to a type 1 model with Lorentzian distribution. The temperature-factor expression is $\exp(-2\pi^2 a^{-2} \sum U_i h_i^2)$. E.s.d.'s are given in parentheses. $S(F_i^2) = [\sum w(F_i^2 - \text{scale} F_i^2)^2 / (n - m)]^{1/2}$; $n = \text{number of observations}$, $m = \text{number of variables}$; $R(F_i) = \sum |F_i - \text{scale} F_i| / \sum F_i$; $wR(F_i^2) = [\sum w(F_i^2 - \text{scale} F_i^2)^2 / \sum w(F_i^2)]^{1/2} = 2wR(F_i)$ [R factors include only $|F_i| > 3\sigma(F_i^2)$]. Compositions given without e.s.d.'s were not refined.

	CoS ₂ (295 K)				NiS ₂ (135 K)				
	Procrystal		Multipole model		Procrystal		Multipole model		
Composition $M:S$	1:2	1:1.97 (1)	1:2	1:1.97	1:2	1:1.968 (6)	1:2	1:1.97	1:1.97
($\sin\theta/\lambda$) range (\AA^{-1})	< 1.49	0.85–1.49	< 1.49	< 1.49	< 1.63	0.85–1.63	< 1.63	< 1.63	< 1.48
Scale	7.29 (1)	7.35 (2)	7.25 (2)	7.36 (2)	6.790 (6)	6.84 (1)	6.74 (1)	6.84 (1)	6.84 (1)
Extinction $G \times 10^4$	0.71 (1)	0.99 (9)	0.73 (1)	0.75 (2)	0.49 (1)	0.67 (4)	0.52 (1)	0.53 (1)	0.52 (1)
y_{min}	0.63	0.96	0.63	0.63	0.65	0.96	0.63	0.63	0.64
$U_{11}(M)$ (\AA^2)	0.00426 (2)	0.00433 (3)	0.00432 (4)	0.00436 (4)	0.002927 (8)	0.00297 (1)	0.00297 (2)	0.00300 (2)	0.00284 (3)
$U_{11}(S)$	0.00001 (1)	0.00001 (1)	–0.00002 (3)	0.00002 (3)	0.00008 (1)	0.00007 (1)	0.00011 (3)	0.00011 (3)	0.00011 (3)
$U_{11}(S)$	0.00453 (2)	0.00441 (4)	0.00446 (3)	0.00446 (3)	0.00296 (1)	0.00284 (2)	0.00287 (2)	0.00287 (2)	0.00287 (2)
$U_{11}(S)$	–0.00016 (2)	–0.00010 (2)	–0.00010 (2)	–0.00010 (2)	–0.00010 (1)	–0.00009 (1)	–0.00007 (1)	–0.00007 (1)	–0.00008 (1)
$x(S)$	0.38988 (1)	0.38986 (2)	0.38987 (1)	0.38987 (1)	0.39453 (1)	0.39453 (1)	0.39454 (1)	0.39454 (1)	0.39454 (1)
$S(F_i^2)$	1.4061	1.1109	1.0468	1.0458	1.2481	1.0567	0.9894	0.9887	0.9856
$R(F)$	0.01461	0.01693	0.01190	0.01189	0.01573	0.01764	0.01361	0.01358	0.01238
$wR(F_i^2)$	0.02722	0.02697	0.01994	0.01993	0.02112	0.02293	0.01657	0.01656	0.01469
$n - m$	736	589	713	713	1106	945	1083	1083	807

of the asphericity of the atoms by means of a sum of multipolar deformation functions $\rho_{nlm\pm} = P_{nlm\pm} \rho_n(r) C_{lm\pm} y_{lm\pm}$ (Stewart, 1976) which are chosen to be equivalent to the deformation functions of Hirshfeld (1977). The terms $y_{lm\pm}$ are real spherical harmonic functions and $C_{lm\pm}$ values are their normalization constants. For both the metal atom M (Co, Ni) and S, three monopolar ($n = 0, 2, 4$), two quadrupolar ($n = 2, 4$) and one set of hexadecapolar ($n = 4$) functions were used. In addition, two dipolar ($n = 1, 3$) and one set of octopolar ($n = 3$) functions were assigned to S, resulting in 8 and 13 population parameters $P_{nlm\pm}$ for M and S, respectively [index-picking rules of site-symmetric spherical harmonics are given by Kurki-Suonio (1977)]. The radial functions are represented by $\rho_n(r) = N_n r^n \exp(-ar)$, where N_n is a normalization constant and a is a refinable parameter common to all functions of an atom. The local Cartesian coordinate systems for the metal and the S atoms are z along [111] and y along $[\bar{1}10]$. All refinements were full-matrix calculations on $|F|^2$ with weights equal to the reciprocal variances of $|F|^2$. The free-atom scattering factors in analytical form were taken from Cromer & Mann (1968) and the dispersion corrections from *International Tables for X-ray Crystallography* (1974, Vol. IV). Convergence of the refinements was considered complete if the ratios full shift/e.s.d. for all parameters were smaller than 10^{-4} . An isotropic secondary-extinction parameter was included in all refinements. Lowest reliability indices for the procrystal model were obtained with the type 1 extinction model adjusting a variable G for the mosaic spread, rather than with the type 2 model using a variable R for the domain size. For the mosaic distribution, a slight preference for the Lorentzian over the Gaussian distribution was obtained. This type of correction was therefore used in all refinements.

To test for deviations from ideal stoichiometry in both compounds, the site occupancy of S was refined

in spherical-atom refinements together with the other parameters. Only data with $(\sin\theta/\lambda) > 0.85 \text{ \AA}^{-1}$ were used to avoid bias from the non-spherical valence density (Table 2). These refinements yielded compositions of $\text{CoS}_{1.97(1)}$ and $\text{NiS}_{1.968(6)}$. For NiS_2 , the refined composition agrees with that derived from the lattice parameter (see *Experimental*); CoS_2 is not otherwise known to be nonstoichiometric.

In the aspherical-atom refinements, larger e.s.d.'s were obtained than in the procrystal refinements, especially for the thermal displacement parameters, although the reliability indices are lower (Table 2). This is due to the more flexible model which, on the one hand, accounts for the obviously significant effects of the asphericity of the atoms, resulting in significantly lower reliability indices; on the other hand, high correlations between refined parameters can result in less precise parameter values than are obtained with models using fewer refinable parameters. Indeed, the e.s.d.'s of highly correlated variables are generally large. High-correlation coefficients were obtained between the following parameters:

$$\begin{aligned} U_{11}(M) - \text{monopoles of } M: & 0.90\text{--}0.91 \text{ for CoS}_2, 0.83\text{--}0.93 \text{ for NiS}_2; \\ U_{11}(S) - \text{monopoles of S:} & 0.81\text{--}0.82 \text{ for CoS}_2, 0.76\text{--}0.77 \text{ for NiS}_2; \\ U_{11}(S) - \text{scale factor:} & 0.93 \text{ for CoS}_2, 0.88\text{--}0.90 \text{ for NiS}_2. \end{aligned}$$

As an example of the dependence of the resulting structural parameters on $(\sin\theta/\lambda)_{\text{max}}$, the following variations of $U_{11}(\text{Ni})$ in NiS_2 are reported: for $(\sin\theta/\lambda)_{\text{max}} < 1.10 \text{ \AA}^{-1}$, $U_{11}(\text{Ni}) = 0.00300(10) \text{ \AA}^2$; $(\sin\theta/\lambda)_{\text{max}} < 1.30 \text{ \AA}^{-1}$, $U_{11}(\text{Ni}) = 0.00290(5) \text{ \AA}^2$; $(\sin\theta/\lambda)_{\text{max}} < 1.35, 1.40, 1.45$ and 1.50 \AA^{-1} , $U_{11}(\text{Ni}) = 0.00284(3) \text{ \AA}^2$; $(\sin\theta/\lambda)_{\text{max}} < 1.63 \text{ \AA}^{-1}$, $U_{11}(\text{Ni}) = 0.00300(2) \text{ \AA}^2$. At $(\sin\theta/\lambda)_{\text{max}} \approx 1.5 \text{ \AA}^{-1}$, the population parameters of the three Ni-monopole functions also change and even reverse their signs (Table 3, last two columns). Accordingly, the highly correlated values of the monopolar populations, the thermal displacement parameters, the scale factor derived from the charge-density refinements and the

Table 3. Multipole populations

Normalization of the deformation functions is such that $\int |\rho_n(r)C_{lm\pm y_{lm\pm}}|d^3r = 1$ for all l and m , including $l=0$. E.s.d.'s in parentheses refer to the last digit given unless indicated otherwise.

	FeS ₂		CoS ₂		NiS ₂	
	(a)	(b)	(a)	(b)	(a)	(b)
Composition M:S	1:1	1:2	1:2	1:1.97	1:1.97	1:1.97
(Sinθ/λ) _{max} (Å ⁻¹)	1.46	1.46	1.49	1.49	1.63	1.48
Reflections included	$F_o^2 > 0$	$F_o^2 > \sigma(F ^2)$	All	All	All	All
M						
P_{000}	0.1 (1)	0.09 (0.11)	0.3 (1)	0.02 (0.14)	0.1 (1)	-0.4 (1)
P_{200}	-0.1 (3)	0.1 (2)	-0.5 (3)	-0.3 (3)	-0.5 (2)	0.8 (2)
P_{400}	0.3 (4)	-0.3 (3)	0.5 (3)	0.2 (3)	0.6 (2)	-0.4 (2)
P_{220}	0.8 (1)	-0.3 (1)	0.09 (0.13)	0.09 (0.13)	-0.2 (1)	-0.2 (1)
P_{420}	0.6 (1)	0.3 (1)	-0.03 (0.10)	-0.03 (9)	0.17 (9)	0.2 (1)
P_{440}	0.46 (5)	0.45 (4)	0.32 (4)	0.32 (4)	0.21 (3)	0.21 (3)
P_{441}	0.12 (5)	0.08 (3)	0.24 (3)	0.24 (3)	0.18 (3)	0.19 (3)
P_{443}	0.58 (5)	0.62 (3)	0.49 (4)	0.48 (3)	0.48 (4)	0.46 (3)
α	11.4 (5)	13.2 (5)	14.8 (7)	14.9 (7)	16.9 (7)	15.8 (7)
S						
P_{000}	0.07 (0.27)	0.3 (2)	0.06 (2)	0.07 (0.17)	0.5 (2)	0.4 (2)
P_{200}	0.5 (9)	-1.4 (1.0)	-0.9 (1.0)	-0.8 (1.0)	-3.7 (2.9)	-4.0 (3.1)
P_{400}	0.6 (9)	1.1 (9)	0.7 (1.0)	0.8 (1.0)	3.1 (3.0)	3.7 (3.3)
P_{110}	0.01 (0.16)	0.01 (0.13)	0.08 (0.11)	0.08 (0.10)	-0.5 (3)	-0.5 (3)
P_{310}	0.3 (8)	0.2 (7)	-1.8 (1.2)	-1.7 (1.1)	-0.5 (9)	-0.8 (1.0)
P_{220}	-0.4 (4)	-0.6 (3)	-1.0 (4)	-1.0 (4)	-1.6 (5)	-1.5 (5)
P_{420}	0.4 (1.3)	0.9 (1.4)	2.8 (2.4)	2.7 (2.3)	7.9 (5.9)	8.0 (6.3)
P_{330}	0.8 (4)	0.6 (3)	0.8 (3)	0.8 (3)	0.8 (4)	0.8 (4)
P_{331}	1.2 (4)	!1 (4)	0.6 (3)	0.6 (3)	1.3 (7)	1.5 (8)
P_{333}	0.2 (2)	0.002 (0.154)	-0.1 (1)	0.1 (2)	0.1 (2)	0.05 (0.15)
P_{440}	0.2 (3)	0.3 (3)	1.0 (5)	1.0 (5)	2.1 (1.1)	2.3 (1.3)
P_{441}	-1.3 (5)	-1.2 (5)	0.2 (2)	0.2 (2)	-1.3 (6)	-1.1 (6)
P_{443}	-0.03 (0.23)	-0.3 (2)	0.07 (0.13)	0.06 (0.13)	-0.1 (2)	-0.1 (2)
α	3.6 (4)	3.5 (3)	3.7 (5)	3.7 (5)	3.3 (4)	3.3 (4)

net charges of the atoms resulting from the refined monopole populations should be interpreted cautiously (Hirshfeld, 1977; Restori & Schwarzenbach, 1986). The other variables, however, are reliably determined and show no significant variations with $(\sin\theta/\lambda)_{\max}$ and stoichiometry (Table 3).

In order to compare the results of the charge-density refinements of CoS₂ and NiS₂ with those of FeS₂, the deposited data of Stevens *et al.* (1980) were refined using the same multipole model as for the other two compounds. The data of FeS₂ had been collected at room temperature up to $(\sin\theta/\lambda)_{\max} = 1.46 \text{ \AA}^{-1}$ with Pd-filtered Ag K α radiation. The deposited $|F_o|$ values had been corrected for isotropic extinction and placed on an absolute scale according to a conventional full-data refinement. The charge-density refinements by Stevens *et al.* were based on $|F|$ and included only reflections with $|F_o|$ and $|F_c|$ larger than $\sigma(|F|)$; we have carried out two refinements on $|F|^2$, one using all reflections with $|F_o|^2 > 0$, the other including only reflections with $|F_o|^2 > \sigma(|F|^2)$. The reliability indices obtained by Stevens *et al.* for their multipole refinement using fixed monopole populations were $R(|F|) = 2.05\%$, $wR(|F|) = 1.62\%$ and $S = 1.68$; those of the present refinements are comparable: $R(|F|) = 2.34$ and 1.76% , $wR(|F|^2) = 3.35$ and 1.92% , $S = 1.31$ and 1.02 for $|F|^2 > 0$ and $|F|^2 > \sigma(|F|^2)$, respectively. The extinction parameter converged to a value close to zero, 0.0001 (1), and the scale factors, 0.998 (3) and 0.995 (2), deviated only slightly from 1. The refined values for the positional and thermal parameters are in fair agreement: Stevens *et al.* Fe: $U_{11} =$

0.00266 (2), $U_{12} = -0.00004$ (2) \AA^2 , S: $U_{11} = 0.00354$ (3), $U_{12} = 0.00007$ (2) \AA^2 , $x = 0.38484$ (2); this refinement $[|F|^2 > \sigma(|F|^2)]$ Fe: $U_{11} = 0.00255$ (3), $U_{12} = 0.00001$ (3) \AA^2 , S: $U_{11} = 0.00312$ (3), $U_{12} = 0.00006$ (1) \AA^2 , $x = 0.38485$ (1).

Results and discussion

Standard structural parameters

For all three compounds, FeS₂, CoS₂ and NiS₂, the positional parameter x of S is almost insensitive to the type of refinement. It even assumes the same value in the procrystal and the aspherical-atom refinements, indicating a negligible asphericity shift of the S atoms. A list of selected bond lengths, bond angles and root-mean-square (r.m.s.) displacements obtained from comparable conventional procrystal refinements is given in Table 4 for FeS₂ (Stevens *et al.*, 1980), CoS₂ (this study), NiS₂ (room temperature: Nowack, Schwarzenbach, Gonschorek & Hahn, 1989; 135 K: this study) and CuS₂ (King & Prewitt, 1979).

The M—S distances increase from FeS₂ to CuS₂ whereas the S—S distances decrease (*cf. Introduction*). In NiS₂, the Ni—S distance increases by 0.0044 (3) \AA from 135 to 295 K, whereas the S—S distance remains nearly constant within 0.0017 (4) \AA . The deviation of the S—M—S angle from 90° is due to the compression of the coordination octahedron of the metal atom along the [111] direction, *i.e.* the threefold axis. The variation of this bond angle shows the decreasing distortion of the octahedron

Table 4. Selected bond lengths, bond angles and r.m.s. displacements

The values were computed from positional and anisotropic displacement parameters of procrystal refinements assuming stoichiometric compositions.

	FeS ₂ (Stevens <i>et al.</i> , 1980)	CoS ₂ (this study)	NiS ₂ (Nowack <i>et al.</i> , 1989)	CuS ₂ (King & Prewitt, 1979)	NiS ₂ (this study)
Temperature (K)	RT	RT	RT	RT	135
Bond lengths (Å)					
M—S	2.2633 (2)	2.3252 (1)	2.3987 (3)	2.4528 (1)	2.3943 (1)
S—S	2.1604 (3)	2.1128 (1)	2.0757 (4)	2.0300 (6)	2.0740 (1)
Bond angles (°)					
∠(S—M—S)*	94.355 (4)	93.945 (3)	93.578 (9)	93.27 (1)	93.585 (2)
∠(S—S—M)	102.33 (1)	103.490 (4)	104.58 (1)	105.52 (2)	104.555 (3)
R.m.s. displacements (Å)					
M					
[111]	0.0505 (9)	0.0654 (2)	0.0782 (9)	0.116 (1)	0.0556 (2)
⊥[111]	0.0517 (6)	0.0652 (2)	0.0738 (6)	0.1090 (8)	0.0534 (1)
(M—S)	0.0513 (5)	0.0653 (2)	0.0751 (4)	0.1111 (5)	0.05401 (8)
S					
[111]	0.057 (1)	0.0649 (3)	0.070 (1)	0.089 (2)	0.0525 (2)
⊥[111]	0.0563 (8)	0.0685 (2)	0.0723 (8)	0.1106 (7)	0.0553 (1)
(M—S)	0.0565 (6)	0.0675 (2)	0.0716 (6)	0.105 (1)	0.05452 (9)
Difference (Å)					
S (M—S) — M (M—S)	0.0052 (8)	0.0023 (3)	−0.0035 (7)	−0.006 (1)	0.0005 (1)

* Only the larger angle of the trigonally compressed octahedron is given, the smaller one being complementary.

from FeS₂ to CuS₂. The environment of the S atoms also comes closer to the ideal tetrahedral geometry in going from FeS₂ to CuS₂ as evidenced by the increasing S—S—M angle.

The r.m.s. displacements of the metal and S atoms parallel and perpendicular to [111] as well as along the M—S bond (Table 4) show that the anisotropy of the atomic displacements is small for both types of atoms in all four compounds. From FeS₂ to CuS₂, thermal motion increases for both metal and S, in agreement with the increasing M—S distances. In particular, we point out the following trends:

(a) From Fe to Cu, the vibrational amplitudes of the metal atoms parallel to [111] increase by larger amounts than those perpendicular to [111]. Whereas in FeS₂, the displacement of the metal atom along [111] is the smaller one of the two quantities, it becomes increasingly the larger one in CoS₂, NiS₂ and CuS₂. This trend cannot be understood using simple geometric arguments. The more compressed the octahedron, the larger is the surface of the octahedral face perpendicular to [111]. Thus, contrary to observation, one might expect that with decreasing distortion of the coordination octahedron the displacement along [111] should become more similar to that perpendicular to [111].

(b) For S, the displacements perpendicular to [111], *i.e.* perpendicular to the direction of the S—S bond, increase more than those parallel to [111]. The vibration parallel to the S—S bond is the larger one in FeS₂, but becomes the smaller one in CoS₂ and NiS₂ and particularly in CuS₂. This trend correlates with the lengthening of the M—S distances which should mainly affect the vibrations perpendicular to [111], the M—S bonds forming angles of 102 to 106° with the S—S bond axes. The displacements along [111] might also be reduced by the strengthening of the S—S bonds in going from FeS₂ to CuS₂,

although the thermal motion of S is probably dominated by rigid-body movements of the S₂ dumb-bell. [The rigid-bond criterion (Hirshfeld, 1976) is necessarily obeyed since the S—S bond passes through a centre of symmetry.]

(c) The vibrational amplitudes of the metal atoms along the directions of the M—S bonds increase by larger amounts than those of the S atoms in going from Fe to Cu; whereas in FeS₂ and CoS₂, the S atoms have the larger amplitudes, the situation is reversed in NiS₂ and CuS₂. This may again be correlated with the lengthening of the M—S distances permitting larger vibrational amplitudes for the metal atoms whereas the vibrations of the S atoms may be limited by the packing of the S₂ anions.

(d) In NiS₂ at 135 K, Ni and S have vibrational amplitudes of the same order of magnitude [$U_{\text{eq}}(\text{Ni}) = 0.00293$ (1), $U_{\text{eq}}(\text{S}) = 0.00296$ (1) Å²], whereas at room temperature, the Ni vibrations exceed those of S by about 10% [$U_{\text{eq}}(\text{Ni}) = 0.00567$ (7), $U_{\text{eq}}(\text{S}) = 0.00511$ (10) Å²]. A similar effect was observed in the isostructural SiP₂ (Chattopadhyay & von Schnering, 1984), where the vibrational amplitudes for Si and P are equal at low temperatures (60, 120 K), but significantly larger for Si than for P at room temperature.

Model maps

In an octahedral crystal field, the lobes of the cubic t_{2g} orbitals are oriented perpendicular to the faces of the coordination octahedron, whereas the lobes of the cubic e_g orbitals are directed towards the vertices. In the pyrite structure, the coordination octahedron of the metal atom has symmetry $\bar{3}$. Two of its faces are perpendicular to the $\bar{3}$ axis; the other six faces are equivalent and oblique to the threefold axis. Concomitantly, the t_{2g} orbitals of cubic sym-

metry are further split into one a_g orbital with its lobes pointing along the threefold axis, and two e'_g orbitals.

Figs. 1(a)–1(d) show sections of the electron density around the metal atoms containing all directions relevant for the study of d orbitals, namely

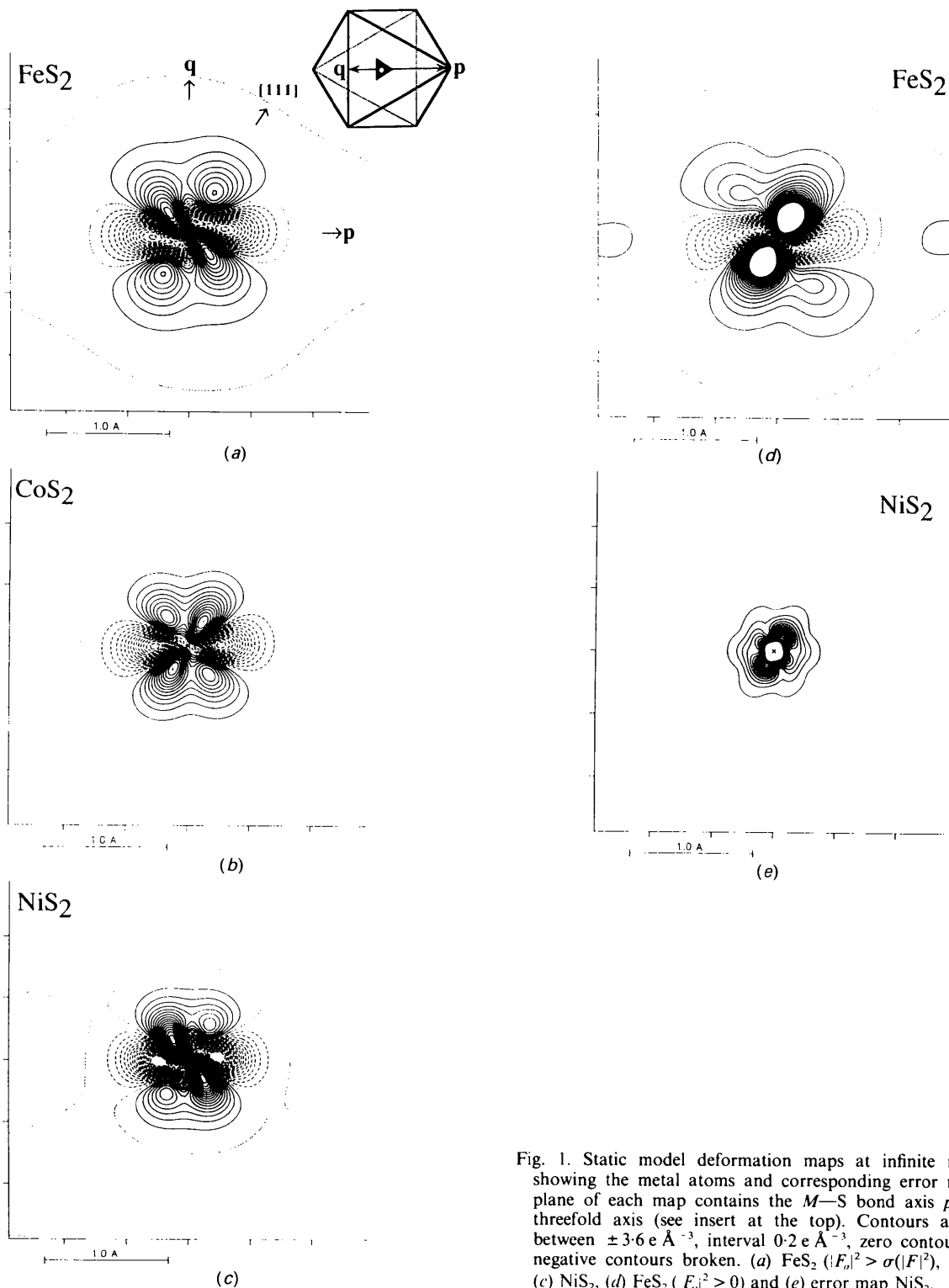


Fig. 1. Static model deformation maps at infinite resolution showing the metal atoms and corresponding error map. The plane of each map contains the M – S bond axis p and the threefold axis (see insert at the top). Contours are drawn between $\pm 3.6 \text{ e } \text{Å}^{-3}$, interval $0.2 \text{ e } \text{Å}^{-3}$, zero contour dotted, negative contours broken. (a) FeS_2 ($|F_o|^2 > \sigma(|F|^2)$), (b) CoS_2 , (c) NiS_2 , (d) FeS_2 ($F_o > 0$) and (e) error map NiS_2 .

the $M-S$ bond axis running horizontally from left to right (but not the S atom itself), the $\bar{3}$ axis, and the normal to one pair of octahedral faces oblique to the $\bar{3}$ axis. The maps were obtained by summation of the deformation functions in direct space. Monopole functions were omitted from the maps because their populations were not determined reliably by the X-ray experiments (see *Least-squares refinements*). Differences in the refinements such as assumed stoichiometry and $(\sin\theta/\lambda)_{\max}$ cut-off had no significant effects on the maps. As for all high-order refinements of heavy-atom compounds, residual maps are quite noisy as evidenced by the relatively high R values.

The deformation densities at the metal-atom sites show maxima pointing towards all octahedral faces, *i.e.* to both those perpendicular to the threefold axis and those of the other kind. On the $M-S$ bond axis, troughs of negative density are observed. All these features are explained by a preferential occupation of the cubic t_{2g} orbitals. The main deviation from cubic symmetry is brought about by very sharp features closer than 0.25 \AA to the metal site which are superimposed on one pair of maxima, either parallel (Figs. 1*b*, 1*d*) or perpendicular (Figs. 1*a*, 1*c*) to the threefold axis. These features are not significant, as can be seen from the error map (Fig. 1*e*) calculated for NiS_2 by summing the variances and covariances of the deformation parameters (Hirshfeld, 1977). The error maps for the other compounds look very similar, the error density reaching $10\text{--}20 \text{ e \AA}^{-3}$ close to the atomic centres. The location of the sharp features on one or the other pair of maxima seems to be accidental. This is also evident by comparing the two

maps of FeS_2 ; Fig. 1(*a*) being obtained from the refinement with $|F_o|^2 > \sigma(|F|^2)$ and Fig. 1(*d*) with $|F_o|^2 > 0$. Hence, whereas the refinements by Stevens *et al.* (1980) indicated that the maxima on the threefold axis are the larger ones, we draw no such conclusions from our maps. The heights of the lower-density maxima are for FeS_2 [$|F_o|^2 > \sigma(|F|^2)$] $1.6(2) \text{ e \AA}^{-3}$ at 0.39 \AA from the atomic centre; for CoS_2 $1.6(2) \text{ e \AA}^{-3}$ at 0.30 \AA ; for NiS_2 $1.2(2) \text{ e \AA}^{-3}$ at 0.32 \AA . The smaller peak height at the Ni site agrees with the expectation that flatter features should be observed for the more electron-rich atom; an atom with completely filled d orbitals would be spherically symmetric. The spatial extension of the d -electron density, as inferred from the $(\pm 0.2 \text{ e \AA}^{-3})$ contour lines of Figs. 1(*a*)–1(*c*), decreases from a radius of 0.85 \AA for Fe to 0.70 \AA for Co, and further to 0.65 \AA for Ni. This reflects the increasing nuclear charges of the atoms.

Fig. 2 shows model maps in the plane x, x, z containing the $M-S$ and the $S-S$ bonds. Monopole functions were included in the calculations of these maps. Along the $M-S$ bond axis, a continuous charge-density bridge of 0.1 e \AA^{-3} is observed for FeS_2 , whereas in CoS_2 and NiS_2 the density appears to be more concentrated around the S atoms as inferred from the (0.1 e \AA^{-3}) contour line. This observation correlates with the increasing $M-S$ distances from FeS_2 to NiS_2 , indicating decreasing metal-sulfur interactions. The e.s.d. in this region amounts to about 0.05 e \AA^{-3} for all three compounds. Thus, the density features are only slightly above the error levels, but those appearing in all three compounds may be significant. In the centre of

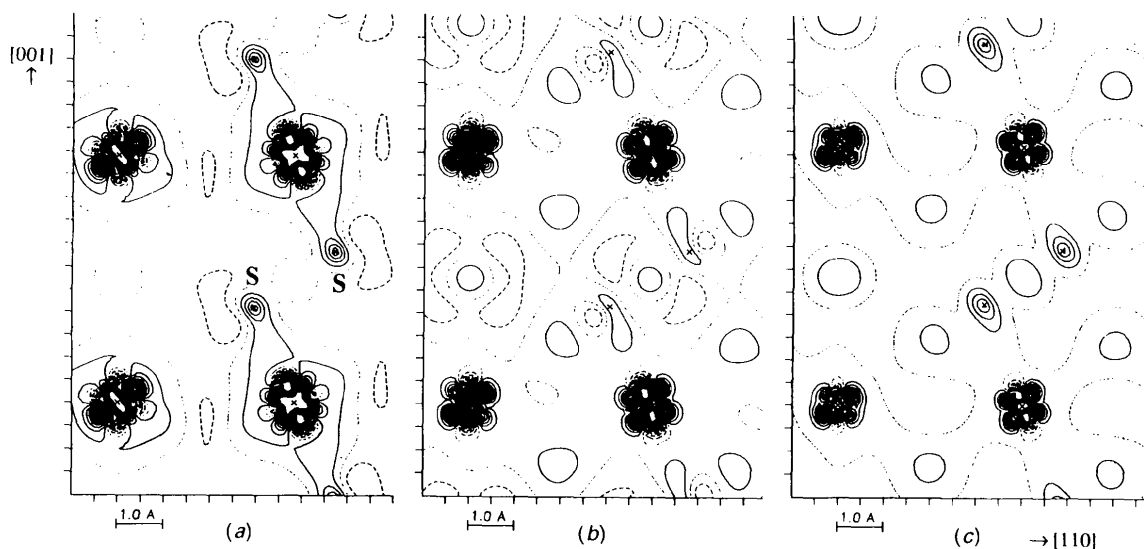


Fig. 2. Static model deformation maps in the plane x, x, z . Contour levels are (a) FeS_2 0.1 e \AA^{-3} , (b) CoS_2 0.1 e \AA^{-3} , (c) NiS_2 0.2 e \AA^{-3} . Atoms in the plane are indicated by crosses, S atoms are labelled in (a).

the S—S bond axis, a small accumulation of electron density is observed which ranges from slightly less than $0.10 \text{ e } \text{Å}^{-3}$ in FeS₂ and $0.15 \text{ e } \text{Å}^{-3}$ in CoS₂ to $0.30 \text{ e } \text{Å}^{-3}$ in NiS₂, the e.s.d. being $0.1 \text{ e } \text{Å}^{-3}$ for all three compounds. Although hardly above the error level, these features agree with the progressive strengthening of the S—S bond indicated by the decreasing S—S distances. On the back sides of the S—S bond, at a distance of 1.3 Å , further small density accumulations of 0.10 (5) and 0.2 (1) $\text{e } \text{Å}^{-3}$ are resolved in CoS₂ and NiS₂ which may be assigned to lone-pair electrons.

d-Orbital occupancies

Holladay, Leung & Coppens (1983) have shown that occupancies of the *d* orbitals of transition-metal atoms can be derived from the multipole parameters. The multipolar density functions centred on a metal atom represent to a good approximation the products of the *d* orbitals if their exponent α is large, and if the contributions of the density functions of neighbouring atoms to the total density near the metal nucleus are negligible. Both density functions and orbital products should assume appreciable values only at distances less than about 1 Å from the metal nucleus. Occupancies of the *d* orbitals in pyrite have been derived by Stevens & Coppens (1979) and Stevens *et al.* (1980).

The crystal field at the site of the metal atom, symmetry $\bar{3}$, splits the *d* orbitals into one a_g and two e_g levels. The electron density of the *d*-orbital products has local symmetry $\bar{3}m$ and is described by five parameters, namely three occupancy factors $P(a_g)$, $P(e_g)$ and $P(e'_g)$, a mixing term $P(e_g, e'_g)$, and an azimuthal angle φ of rotation about the $\bar{3}$ axis indicating the position of the local mirror plane. The corresponding observed electron density is characterized by five density-function population parameters, namely $P_{00} = P + P_{000} + P_{200} + P_{400}$, $P_{20} = P_{220} + P_{420}$, $P_{40} = P_{440}$, $P_{43+} = P_{443+}$ and $P_{43-} = P_{443-}$, P being the number of valence electrons in the neutral atom. The observed φ angle between the x axis of the local coordinate system used for the refinement and the nearest local mirror plane of $\bar{3}m$ of the *d*-orbital products is computed from $\tan(3\varphi) = P_{43-}/P_{43+}$ (Holladay *et al.*, 1983). A rotation of the coordinate system by φ placing x' into, and y' perpendicular to the mirror plane gives $P'_{43+} = (P_{43+}^2 + P_{43-}^2)^{1/2}$ and $P'_{43-} = 0$. The observed populations $P(a_g)$, $P(e_g)$, $P(e'_g)$ and $P(e_g, e'_g)$ are obtained from P_{00} , P_{20} , P_{40} and P'_{43+} by a linear transformation (Paturle & Coppens, 1988). The values assumed by $P(e_g)$, $P(e'_g)$ and $P(e_g, e'_g)$ depend on the particular choice of the e_g and e'_g orbitals. Any unitary transformation of the orbitals $e(x'y')$, $x'^2 - y'^2$ and $e(x'z, y'z)$ results in a different set of values. [$e(x'y')$,

Table 5. *d-Orbital occupancies*

Model (I) assumes M^{2+} ions, d^6 , d^7 and d^8 for Fe, Co and Ni, respectively; model (II) assumes $P(a_g) = 2$. $\delta\varphi$ is the angle between the local mirror planes of the coordination polyhedron and those of the *d*-electron density. The multipole populations are taken from refinements (b) of FeS₂, (b) of CoS₂ and (a) of NiS₂ (see Table 3). E.s.d.'s computed with the variances and covariances obtained from least squares are given in parentheses.

Model		FeS ₂	CoS ₂	NiS ₂
(I), (II)	$\delta\varphi$ (°)	0.1 (1.0)	4.9 (1.2)	1.7 (1.0)
	$2P(a_g) - P(e'_g)$	0.04 (8)	0.05 (9)	-0.21 (8)
	$P(e_g, e'_g)$	0.11 (7)	-0.11 (9)	-0.10 (8)
(I)	$P(a_g)$	1.50 (4)	1.65 (4)	1.74 (3)
	$P(e_g)$	2.96 (4)	3.25 (4)	3.68 (4)
	$P(e'_g)$	1.54 (4)	2.10 (4)	2.58 (4)
(II)	$P(a_g)$	2.00	2.00	2.00
	$P(e'_g)$	3.96 (8)	3.95 (9)	4.21 (8)
	$P(e_g)$	2.54 (8)	2.80 (8)	3.10 (8)

$x'^2 - y'^2$) is composed of $x'y'$ and $x'^2 - y'^2$ orbitals, and $e(x'z, y'z)$ of $x'z$ and $y'z$ orbitals, where x' , y' , z are coordinates in the rotated local coordinate system.] In particular, one such transformation results in $P(e_g, e'_g) = 0$. Since the symmetry of the coordination of the metal by S is nearly cubic, we choose e_g and e'_g in such a way that they show the deviation from exact cubic symmetry: $e_g = -(2/3)^{1/2}e(x'z, y'z) + (1/3)^{1/2}e(x'^2 - y'^2, -x'y')$, $e'_g = (1/3)^{1/2}e(x'z, y'z) + (2/3)^{1/2}e(x'^2 - y'^2, -x'y')$. For exact cubic symmetry, a_g and e'_g merge into t_{2g} , $2P(a_g) - P(e'_g) = 0$ and $P(e_g, e'_g) = 0$; in addition, the local mirror planes of the *d*-electron density coincide with the mirror planes of the coordination octahedron, the latter passing through the metal and two S atoms.

As has been described above, the values obtained for the number of valence electrons of the metal atom P_{00} depend on the type of refinement (Table 3); they are correlated with the displacement parameters, the scale factor, and through the neutrality constraint with the monopolar population parameters of S. Believing that populations of monopolar deformation functions do not represent physically meaningful atomic charges, we treat P_{00} as an unknown quantity. We consider two different models:

(I) Fe, Co and Ni are all doubly charged cations; P_{00} is thus 6, 7 and 8, respectively.

(II) $P(a_g) = 2$ for all three compounds since a_g is the orbital with lowest energy.

Table 5 shows the resulting orbital populations. The deviations of the electron distributions of the metal atoms from cubic symmetry are, with few exceptions, of the order of the corresponding e.s.d.'s, and never larger than 4 e.s.d.'s: the angle $\delta\varphi$ between the local mirror planes of the coordination polyhedron and those of the *d*-electron density, the value of $2P(a_g) - P(e'_g)$ responsible for the difference of the heights of the electron-density maxima on the octahedral faces, and the mixing term $P(e_g, e'_g)$ are all

close to zero. The results of model (II), in contrast to those of model (I), suggest a very straightforward interpretation. The cubic t_{2g} orbitals are fully occupied in all three compounds by $P(a_g) + P(e'_g) \approx 6$ electrons. The population of the cubic e_g orbitals is larger than for an isolated M^{2+} ion. This may be the result of the covalent overlap between the metal and the S atoms (see *Introduction*), indicating the limitations of both crystal-field theory as applied to pyrite-type structures and orbital-population analysis of diffraction data. In agreement with the increasing $M-S$ distances, both models (I) and (II) show an increase in the population of the antibonding e_g orbital. However, we do not believe that the numerical values have a significance beyond this trend.

Concluding remarks

The results of this study consistently agree with the basic principles of transition-metal chemistry. In all three compounds, the metal atoms are in the low-spin state. This results in important and compact non-spherical electron-density features which can be determined from diffraction data in spite of the fact that the procystal model is often quite appropriate for simple heavy-atom structures such as pyrite and generally permits the attainment of very low agreement factors. The heavier the metal atom, the more compact is the d -electron difference density. Thus, in NiS_2 all features of interest are within a sphere of radius 0.65 Å around the nucleus of Ni. Their observation requires diffraction data of very high resolution. The success of similar studies on heavier atoms may be limited by the resolution attainable, and by difficulties of deconvolution from harmonic and anharmonic thermal displacements and uncertainties in the dispersion correction at large $\sin\theta/\lambda$.

The difference density near the metal atom is the only important feature in all maps. Densities near S are very low and of limited information value. In agreement with cyclic octasulfur (Coppens, Yang, Blessing, Cooper & Larsen, 1977) and the peroxide ion (Savariault & Lehmann, 1980), the difference density between bonded S atoms is indeed very small. In contrast, a pronounced charge accumulation is observed in the centre of the much stronger P—P bond of the isostructural SiP_2 (Chattopadhyay & von Schnering, 1984).

The authors wish to thank Dr Walter Gonschorek for the initial work in this project and valuable discussions. Support of this work by the Swiss

National Science Foundation is gratefully acknowledged.

References

- BECKER, P. J. & COPPENS, P. (1974). *Acta Cryst.* **A30**, 129–147.
 BECKER, P. J. & COPPENS, P. (1975). *Acta Cryst.* **A31**, 417–425.
 BITHER, T. A., BOUCHARD, R. J., CLOUD, W. H., DONOHUE, P. C. & SIMONS, W. J. (1968). *Inorg. Chem.* **7**, 2208–2220.
 BOND, W. L. (1951). *Rev. Sci. Instrum.* **52**, 344–345.
 BULLETT, D. W. (1982). *J. Phys. C*, **5**, 6163–6174.
 CHATTOPADHYAY, T. P. & VON SCHNERING, H. G. (1984). *Z. Kristallogr.* **167**, 1–12.
 COPPENS, P., YANG, Y. W., BLESSING, R. H., COOPER, W. F. & LARSEN, F. K. (1977). *J. Am. Chem. Soc.* **99**, 760–766.
 CROMER, D. T. & MANN, J. B. (1968). *Acta Cryst.* **A24**, 321–324.
 DENNE, W. A. (1977). *Acta Cryst.* **A33**, 438–440.
 DWIGGINS, C. W. (1975). *Acta Cryst.* **A31**, 395–396.
 FLACK, H. D. & VINCENT, M. G. (1978). *Acta Cryst.* **A34**, 489–491.
 FRENCH, S. & OATELY, S. (1982). *Crystallographic Statistics*, edited by S. RAMASESHAN, M. F. RICHARDSON & A. J. C. WILSON, pp. 19–51. Bangalore: Indian Academy of Sciences.
 GOODENOUGH, J. B. (1971). *J. Solid State Chem.* **3**, 26–38.
 HIRSHFELD, F. L. (1976). *Acta Cryst.* **A32**, 239–244.
 HIRSHFELD, F. L. (1977). *Isr. J. Chem.* **16**, 226–229.
 HOLLADAY, A., LEUNG, P. & COPPENS, P. (1983). *Acta Cryst.* **A39**, 377–387.
 HUBBARD, J. (1964). *Proc. R. Soc. London Ser. A*, **281**, 401–419.
 KAUTZ, R. L., DRESSELHAUS, M. S., ADLER, D. & LINZ, A. (1972). *Phys. Rev. B*, **6**, 2078–2082.
 KIKUCHI, K., MIYADAI, T., FUKUI, T., ITÔ, H. & TAKIZAWA, K. (1978). *J. Phys. Soc. Jpn.* **44**, 410–415.
 KING, H. E. & PREWITT, C. T. (1979). *Am. Mineral.* **64**, 1265–1271.
 KJESKUS, A. & NICHOLSON, D. G. (1971). *Acta Chem. Scand.* **25**, 866–876.
 KRABBES, G. & OPPERMAN, H. (1984). *Z. Anorg. Allg. Chem.* **511**, 19–32.
 KRILL, G., LAPIERRE, M. F., GAUTIER, F., ROBERT, C., CZJZEK, G., FINK, J. & SCHMIDT, H. (1976). *J. Phys. C*, **9**, 761–782.
 KURKI-SUONIO, K. (1977). *Isr. J. Chem.* **16**, 115–123.
 LAUER, S., TRAUTWEIN, A. X. & HARRIS, F. E. (1984). *Phys. Rev. B*, **29**, 6774–6783.
 MOTT, N. F. (1961). *Philos. Mag.* **6**, 287–309.
 NOWACK, E., SCHWARZENBACH, D., GONSCHOREK, W. & HAHN, TH. (1989). *Z. Kristallogr.* **186**, 213–215.
 PATURLE, A. & COPPENS, P. (1988). *Acta Cryst.* **A44**, 6–7.
 RESTORI, R. & SCHWARZENBACH, D. (1986). *Acta Cryst.* **B42**, 201–208.
 SAVARIAULT, J.-M. & LEHMANN, M. S. (1980). *J. Am. Chem. Soc.* **102**, 1298–1303.
 SCHLEGEL, A. & WACHTER, P. (1976). *J. Phys. C*, **9**, 3363–3369.
 SHANNON, R. D. (1976). *Acta Cryst.* **A32**, 751–767.
 STEVENS, E. D. & COPPENS, P. (1979). *Acta Cryst.* **A35**, 536–539.
 STEVENS, E. D., DELUCIA, M. L. & COPPENS, P. (1980). *Inorg. Chem.* **19**, 813–820.
 STEWART, J. M., KRUGER, G. J., AMMON, H. L., DICKINSON, C. & HALL, S. R. (1972). The XRAY system – version of June 1972. Tech. Rep. TR-192. Computer Science Center, Univ. of Maryland, College Park, Maryland, USA.
 STEWART, R. F. (1976). *Acta Cryst.* **A32**, 565–574.
 VAUGHAN, D. J. & CRAIG, J. R. (1978). *Mineral Chemistry of Metal Sulfides*. Cambridge Univ. Press.
 WILSON, J. A. & PITT, G. D. (1971). *Philos. Mag.* **23**, 1297–1310.